Ultrafast dynamics of liquid water: Frequency fluctuations of the OH stretch and the HOH bend

ARTICLE *in* THE JOURNAL OF CHEMICAL PHYSICS · JULY 2013

Impact Factor: 2.95 · DOI: 10.1063/1.4813071 · Source: PubMed

3 AUTHORS, INCLUDING:

Sotiris S Xantheas
Pacific Northwest National Laboratory
178 PUBLICATIONS **7,759** CITATIONS
SEE PROFILE

Shinji Saito
Institute for Molecular Science
74 PUBLICATIONS **3,348** CITATIONS
SEE PROFILE

Ultrafast dynamics of liquid water: Frequency fluctuations of the OH stretch and the HOH bend

Sho Imoto,[1] Sotiris S. Xantheas,[2] and Shinji Saito[1,3,a)]
[1]*The Graduate University for Advanced Studies, Myodaiji, Okazaki, Aichi 444-8585, Japan*
[2]*Physical Sciences Division, Pacific Northwest National Laboratory, 902 Battelle Boulevard, P.O. Box 999, MS K1-83, Richland, Washington 99352, USA*
[3]*Department of Theoretical and Computational Molecular Science, Institute for Molecular Science, Myodaiji, Okazaki, Aichi 444-8585, Japan*

(Received 16 May 2013; accepted 21 June 2013; published online 22 July 2013)

Frequency fluctuations of the OH stretch and the HOH bend in liquid water are reported from the third-order response function evaluated using the TTM3-F potential for water. The simulated two-dimensional infrared spectra of the OH stretch are similar to previously reported theoretical results. The present study suggests that the frequency fluctuation of the HOH bend is faster than that of the OH stretch. The ultrafast loss of the frequency correlation of the HOH bend is due to the strong couplings with the OH stretch as well as the intermolecular hydrogen bond bend. © *2013 AIP Publishing LLC*. [http://dx.doi.org/10.1063/1.4813071]

I. INTRODUCTION

Water is associated with various anomalous properties[1] and its structure and dynamics have been intensively investigated both experimentally and theoretically.[2–4] The dynamics of water are characterized by a hydrogen bond (HB) network fluctuating with a wide range of time scales ranging from femto-seconds to several pico-seconds.[5]

The dynamics of water has been experimentally probed using various spectroscopic methods.[6–10] In particular, the infrared (IR) spectrum of the OH stretch has been extensively studied. It is known that the OH stretch is sensitive to its local environment since the frequency of the OH stretch correlates with the strength of the underlying HB. However, information obtained from linear spectroscopy is limited and, thus, the detailed dynamics of the HB network cannot be fully resolved. Nonlinear spectroscopy can be employed to analyze the details of the frequency fluctuations.[11,12] In particular, third-order nonlinear IR spectroscopy, e.g., two-dimensional (2D) IR spectra, has been used to provide detailed information about the dynamics of the OH stretch.[13,14] The frequency correlations of the probe OH (OD) stretch in liquid D_2O (H_2O) show a fast decay with a 60 fs time constant due to the librational motion, a recursion with a 130 fs time constant because of the HB stretch, and a slow decay with a 1 ps time constant arising from the HB rearrangement. In addition, the 2D IR spectra indicate the inhomogeneous frequency fluctuation of the OH stretch in liquid D_2O due to the difference of the HB strength.[15,16] It is also known that the frequency fluctuation of the OH stretch in neat water is quite fast, less than 50 fs, due to strong inter- and intra-molecular couplings.[17,18]

The 2D IR spectra of the OH stretch have also been studied theoretically. It was found that the frequency fluctuation of the OH stretch in liquid D_2O is correlated to the fluctuation of the electric field along the OH bond.[19,20] Furthermore, it was shown that the molecular reorientation coupled with HB exchange is responsible for the long time decay of the frequency correlation with a time constant of 1 ps.[21] The 2D IR spectra of the OH stretch in liquid water have been calculated using a numerical integration of the Schrödinger equations and it was also shown that the spectral diffusion after 200 fs arises from the intermolecular coupling between the OH stretching motions.[22–24]

In contrast to the OH stretch, the HOH bend has not been extensively studied. The time scale of the frequency fluctuation of the HOH bend has not been analyzed to-date either theoretically or experimentally. The scarcity of the theoretical studies regarding the HOH bend can be in part attributed to the difficulty in reproducing its properties. For example, simple model potentials cannot reproduce the increase of the average HOH angle between the gas and condensed phases.[25]

In this study we report the frequency fluctuations of the OH stretch and the HOH bend in liquid water by analyzing the 2D IR spectra calculated from molecular dynamics (MD) simulations. These MD simulations were performed with the *ab initio*-based, flexible, polarizable, transferable TTM3-F potential, which incorporates an intramolecular charge transfer depending on the environment and correctly reproduces the trends of both the HOH bend and the OH stretch in liquid water and ice.[26–28] The 2D IR spectra were evaluated directly from the third-order response function, instead of using the frequency-frequency time correlation function, $\langle \delta\omega(0)\delta\omega(t)\rangle$. Although we employed the high-temperature approximation, the inter- and intra-molecular couplings are explicitly taken into account in the present analysis.

The calculated 2D IR spectra of the OH stretch show the fast decay of the frequency correlation: an initial decay with a time constant of ∼40 fs, a plateau from 60 to 100 fs, and a slow decay with a time constant of ∼180 fs. The frequency fluctuation of the OH stretch is due to the couplings with the HB stretch at ∼200 cm^{-1} and the librational

a)Author to whom correspondence should be addressed. Electronic mail: shinji@ims.ac.jp.

motion as suggested during previous experimental and theoretical studies.[18,22–24] In contrast, the frequency correlation of the HOH bend mainly decreases with a time constant less than 100 fs, exhibits a plateau from 100 to 150 fs, and decays with a time constant of ∼120 fs. We found that the frequency fluctuation of the HOH bend is caused by the strong couplings with the OH stretch as well as the intermolecular HB bend at ∼60 cm^{-1}.

In Sec. II we briefly describe the theoretical background of the third-order IR spectroscopy and details of MD simulations. In Sec. III we present the 2D IR spectra of the OH stretch and the HOH bend and the analysis of those frequency fluctuations. Final conclusions are given in Sec. IV.

II. THEORETICAL METHOD AND COMPUTATIONAL DETAILS

Most theoretical calculations of the third-order response function are based on mapping the electric field onto the vibrational frequency and employing Gaussian statistics for the frequency fluctuation.[12] During previous theoretical studies of the 2D IR spectra of the OH stretch in liquid water, the inter-OH stretch coupling was considered, however the coupling between the OH stretch and the HOH bend has not been taken into account.[22–24] In the present study we calculate directly the third-order response function from non-equilibrium MD simulations. The details of the theoretical calculation of the third-order response function and corresponding spectra from non-equilibrium MD simulations are summarized in Ref. 29. Here, we briefly describe the theoretical background and computational details for third-order nonlinear IR spectroscopy.

Third-order IR spectroscopy measures the third-order polarization, $P^{(3)}(\tau, T, t)$, which is expressed by the convolution of the third-order response function, $R^{(3)}(t_1, t_2, t_3)$, with the electric field as[11]

$$\begin{aligned} &P^{(3)}(\tau, T, t) \\ &= \int_0^\infty dt_3 \int_0^\infty dt_2 \int_0^\infty dt_1 E(t_s - t_3, \{\tau_i\}) E(t_s - t_3 - t_2, \{\tau_i\}) \\ &\quad \times E(t_s - t_3 - t_2 - t_1, \{\tau_i\}) R^{(3)}(t_1, t_2, t_3), \end{aligned} \tag{1}$$

where

$$\begin{aligned} E(t, \{\tau_i\}) = \sum_{i=1}^{3} \varepsilon_i (t - \tau_i) \exp(-i\omega_i (t - \tau_i)) \\ \times \exp(-i\mathbf{k}_i \mathbf{r}_i) + \text{c.c.} \end{aligned} \tag{2}$$

Here, τ_1, τ_2, and τ_3 are the times of the centers of pulses and the three time intervals are defined as $\tau = \tau_2$-τ_1, $T = \tau_3$-τ_2, and $t = t_s$-τ_3. The ω_i, $\mathbf{k}_i$, and $\varepsilon_i(t)$ are the carrier frequency, wave vector, and envelope function of the pulse i, respectively. Equation (1) can be written as

$$P^{(3)}(\tau, T, t) = \sum_{\alpha=\mathrm{I}}^{\mathrm{IV}} \exp(-i\mathbf{k}_\alpha \mathbf{r}) P_\alpha^{(3)}(\tau, T, t) + \text{c.c.}, \tag{3}$$

where $P_{\mathrm{I}}^{(3)}$, $P_{\mathrm{II}}^{(3)}$, $P_{\mathrm{III}}^{(3)}$, and $P_{\mathrm{IV}}^{(3)}$ denote the third-order polarizations generated in the $\mathbf{k}_{\mathrm{I}} = -\mathbf{k}_1 + \mathbf{k}_2 + \mathbf{k}_3$, $\mathbf{k}_{\mathrm{II}} = \mathbf{k}_1 - \mathbf{k}_2 + \mathbf{k}_3$, $\mathbf{k}_{\mathrm{III}} = \mathbf{k}_1 + \mathbf{k}_2 - \mathbf{k}_3$, and $\mathbf{k}_{\mathrm{IV}} = \mathbf{k}_1 + \mathbf{k}_2 + \mathbf{k}_3$ phase matching conditions, respectively.

The third-order response function is given by[11]

$$\begin{aligned} R^{(3)}(t_1, t_2, t_3) = \left(\frac{i}{\hbar}\right)^3 \mathrm{tr}\{\mathbf{M}(t_1 + t_2 + t_3) \\ \times [\mathbf{M}(t_1 + t_2), [\mathbf{M}(t_1), [\mathbf{M}(0), \rho_{\mathrm{eq}}]]]\}, \end{aligned} \tag{4}$$

where ρ_{eq} and $\mathbf{M}$ are the equilibrium density matrix and dipole operator of the system, respectively. By using the identity[30] with the Liouville operator for the system-field interaction,

$$\frac{i}{\hbar}[\mathbf{M}(t),] \equiv i L_{\mathbf{M}}(t) = \lim_{\epsilon \to 0} \frac{1}{\epsilon} \{\exp(i\epsilon L_{\mathbf{M}}(t)) - 1\}, \tag{5}$$

the third-order response function can be recast in the from

$$\begin{aligned} &R^{(3)}(t_1, t_2, t_3) \\ &= \lim_{\epsilon \to 0} \frac{1}{\epsilon^2} \mathrm{tr}\{\mathbf{M}(t_1 + t_2 + t_3)(\exp(i\epsilon L_{\mathbf{M}}(t_1 + t_2)) - 1) \\ &\quad \times (\exp(i\epsilon L_{\mathbf{M}}(t_1)) - 1) \frac{i}{\hbar}[\mathbf{M}(0), \rho_{eq}]\}. \end{aligned} \tag{6}$$

By applying a classical approximation, we obtain the classical expression for the third-order response function based on non-equilibrium MD simulations expressed as[31]

$$\begin{aligned} R^{(3)}(t_1, t_2, t_3) &\propto \langle \mathbf{M}(t_1 + t_2 + t_3) \dot{\mathbf{M}}(0) \rangle_{t_1, t_2} \\ &+ \langle \mathbf{M}(t_1 + t_2 + t_3) \dot{\mathbf{M}}(0) \rangle_{\bar{t}_1, \bar{t}_2} \\ &- \langle \mathbf{M}(t_1 + t_2 + t_3) \dot{\mathbf{M}}(0) \rangle_{\bar{t}_1, t_2} - \langle \mathbf{M}(t_1 + t_2 + t_3) \dot{\mathbf{M}}(0) \rangle_{t_1, \bar{t}_2}. \end{aligned} \tag{7}$$

Here $\langle\ \rangle$ indicates the ensemble average, the subscripts of each term denote the time of the application of external pulses as the perturbation and the over-bar on the subscripts represents the opposite direction of external pulse based on inverted force method.[32]

We used the TTM3-F interaction potential, which is the latest version of the *ab initio*-based charge transferable, flexible, polarizable Thole-Type Models (TTM) to describe the underlying inter- and intra-molecular interactions in liquid water.[26–28,33–38] The details of the TTM3-F potential are presented in Ref. 27. The intramolecular interaction and charge transfer of the TTM3-F potential are based on the monomer potential and dipole moment surfaces obtained from high level *ab initio* calculations,[39] appropriately modified to describe the liquid phase.[27] Because of the intramolecular charge transfer feature, the TTM3-F potential reproduces the increase of the HOH angle in the condensed phase[26] with respect to the gas phase monomer and the correct IR spectrum of the HOH bend. Four interaction sites are used for the intermolecular interaction in the TTM3-F potential. The oxygen-oxygen interaction is described by a Buckingham expotential-6. A positive charge is placed on each hydrogen atom and a negative charge and an isotropic point dipole moment are placed on the M-site located on the bisector of the HOH angle. The Thole type damping function is employed for the treatment of the electrostatic interaction.[40]

All the MD simulations have been performed under the constant volume and energy conditions at a temperature of 300 K and a density of 1.0 g/cm^3. Periodic boundary conditions were employed and the long-range electric

interactions were calculated using the Ewald sum. The induced dipole moment was computed iteratively at each step with a convergence criterion of $|(\mu_{i,N} - \mu_{i,N-1}/\mu_{i,N}| < 1 \times 10^{-10}$, where $\mu_{i,N}$ is the induced dipole moment of molecule i at the N th iteration. Equations of motion were integrated using the velocity-Verlet algorithm with the time step of 0.1 fs, which is needed to solve the linear equations for the induced dipole moment.[38] Equilibrium MD simulations and normal mode analysis of the whole system were carried out using 125 water molecules. The total length of the trajectories was 500 ps. The normal mode analysis was performed every 1 fs along the equilibrium trajectories by using a five-point differentiation of the analytical force.

Non-equilibrium MD simulations were carried out for a system with 64 water molecules. We apply the δ-function-like triangular short external fields, whose intensity and time duration are 1.2 V/Å and 0.2 fs, to calculate the third-order response function shown in Eq. (7). The average temperature rise due to the perturbative δ-function-like pulses was approximately 10 K during each non-equilibrium MD simulation. In order to calculate $P_{\mathrm{i}}^{(3)}$ in Eq. (3), Gaussian functions were used for the envelope function in Eq. (2),

$$\varepsilon_i(t) = \frac{1}{\sqrt{2\pi}\sigma_i}\exp\left(-\frac{t^2}{2\sigma_i^2}\right), \tag{8}$$

where σ_i and ω_i were 40 fs and 1600 cm^{-1} for the HOH bend and 20 fs and 3500 cm^{-1} for the OH stretch. The third-order response function for $t_1 \leq 400$ fs and $t_3 \leq 400$ fs is used for the calculation of the 2D IR spectra. The 2D IR spectra were obtained by averaging over 320 000 trajectories for $t_2 < 100$ fs, 640 000 trajectories for $t_2 < 150$ fs, 1 280 000 trajectories for $t_2 < 300$ fs, and 2 560 000 trajectories for $t_2 < 500$ fs.

III. RESULTS AND DISCUSSION

The 2D IR spectrum is expressed using $P_{\mathrm{I}}^{(3)}(\tau, T, t)$ and $P_{\mathrm{II}}^{(3)}(\tau, T, t)$ as[41]

$$\begin{aligned} S(\omega_1, T, \omega_3) &= \mathrm{Re}\int_0^\infty dt \int_0^\infty d\tau \exp(i(\omega_1\tau - \omega_3 t)) i P_{\mathrm{I}}^{(3)}(\tau, T, t) \\ &\quad + \mathrm{Re}\int_0^\infty dt \int_0^\infty d\tau \exp(i(\omega_1\tau + \omega_3 t)) i P_{\mathrm{II}}^{(3)}(\tau, T, t). \end{aligned} \tag{9}$$

The 2D IR spectra are sensitive to the correlation of the two vibrational frequencies, ω_1 and ω_3, separated by the waiting time T. When T is shorter than the time scale of the frequency fluctuation, the 2D IR spectra are elongated to the diagonal direction because of the strong correlation between ω_1 and ω_3. In contrast, when T is longer than the time scale of the frequency fluctuation, the two frequencies lose their correlation and in that case the 2D IR spectra become parallel to ω_1 axis. That is, the slope of the 2D IR spectra is correlated to the extent of the initial inhomogeneity.

The 2D IR spectra have positive and negative peaks.[12] The positive peak originates from the ground state bleach and the stimulated emission in which both ω_1 and ω_3 correspond to the $0 \rightarrow 1$ transition. In contrast, the negative peak arises from the excited state absorption and ω_1 and ω_3 correspond to the $0 \rightarrow 1$ and $1 \rightarrow 2$ transitions, respectively. The difference in ω_3 for the positive and negative peaks corresponds to the difference in the frequencies of the $0 \rightarrow 1$ and $1 \rightarrow 2$ transitions, i.e., the vibrational anharmonicity.[42] The dynamics in the present analysis are governed by classical mechanics and for this reason no discrete states exist. The frequencies in the present 2D IR spectra are related to those of the fluctuation of the dipole moment obtained from the trajectories perturbed by the electric fields, such as in the conventional IR and sum frequency generation spectra calculated from classical MD simulations.[43,44]

Figure 1(a) shows the 2D IR spectra of the OH stretch. The 2D IR spectra of the OH stretch are diagonally elongated at $T = 0$ fs, indicating the strong correlation between ω_1 and ω_3. The vibrational anharmonicity of the OH stretch estimated from the difference of ω_3 between the positive and negative peaks is 240 cm^{-1}, which is in good agreement with the experimental result of 250 cm^{-1}.[18] Although the spectral shape is rather elliptic at $T = 0$ fs, it becomes egg-shaped at $T = 50$ fs due to the increase/decrease in the peak intensity at (ω_1, ω_3) = (3400 cm^{-1}, 3700 cm^{-1})/(3200 cm^{-1}, 3600 cm^{-1}). This change in the spectral shape arises from the heterogeneous dynamics of the local HB network as experimentally observed in Ref. 13. In addition, the diagonal width decreases and the anti-diagonal width increases with increasing the waiting time T and then both the positive and negative peaks have an almost round shape at $T > 200$ fs similarly to the previous theoretical calculations.[22–24] As in the other theoretical results, however, the rapid decay of the negative peak observed in the experiments[17,18] is not found in the present study either.

To quantify the time scale of the frequency fluctuations, the slope of the 2D IR spectra of the OH stretch was examined. As seen by the red line in Figure 2, the waiting time dependence of the slope consists of the following three processes: an initial decay with a time constant of ~40 fs, a plateau from 60 to 100 fs, and a slow decay with a time constant of ~180 fs. A similar temporal behavior was previously seen in the frequency-frequency time correlation function in Ref. 24. In particular, the third process in liquid water is quite faster than those in liquid D_2O because of the inter- and intramolecular resonances.

Figure 1(b) shows the 2D IR spectra of the HOH bend. The slope of the 2D IR spectrum of the HOH bend at $T = 0$ fs is small compared to that of the OH stretch, which indicates a significant fast frequency fluctuation of the HOH bend. The frequency difference between the positive and negative peaks shows that the vibrational anharmonicity of the HOH bend is 60 cm^{-1}, which is slightly larger than the experimental result of 40 cm^{-1}.[45] The spectra change to a round shape with increasing T and become parallel to the ω_1 axis at $T = 400$ fs. In addition, the change of the spectral shape to the egg-shape seen in the 2D IR spectra of the OH stretch is not clearly seen in the time evolution of the 2D IR spectra of the HOH bend, a result suggesting that the frequency of the HOH bend is less sensitive to the local HB environment than that of the OH stretch.

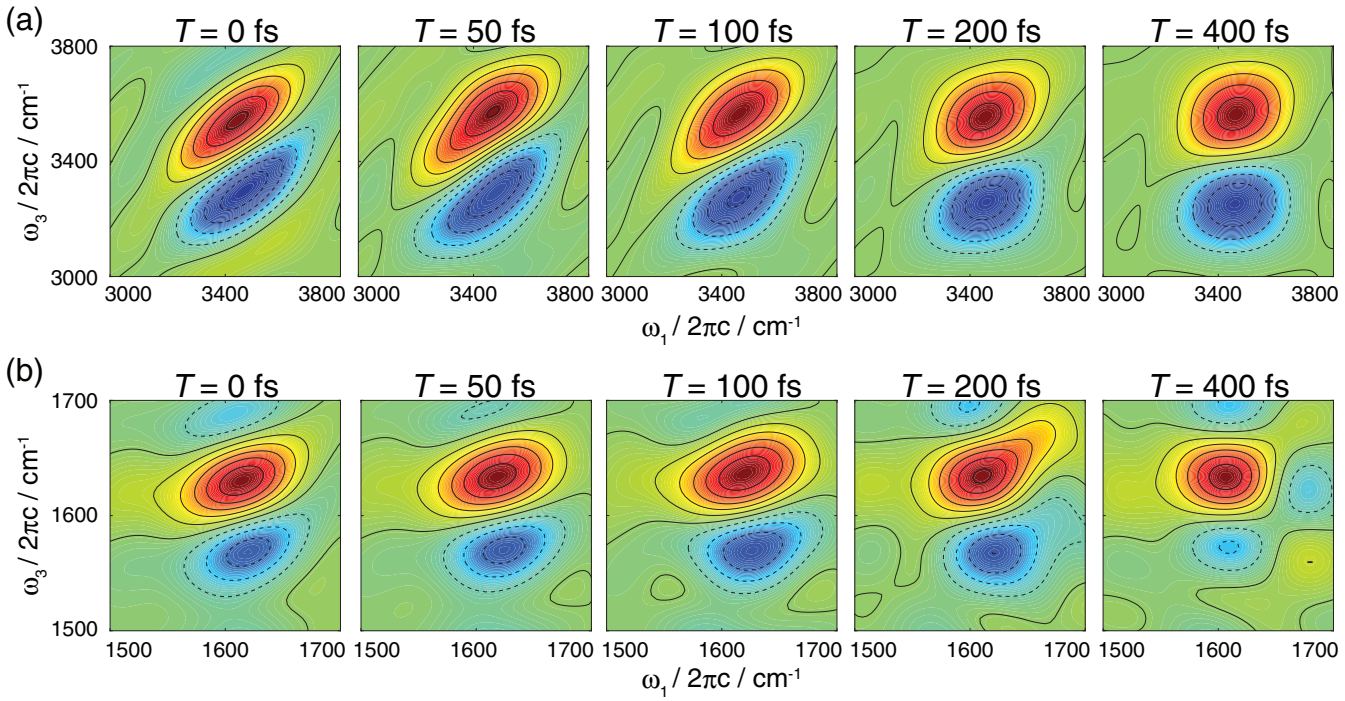

FIG. 1. 2D IR spectra as a function of waiting time for (a) the OH stretch and (b) the HOH bend in liquid water. The spectra are normalized by the maximum value.

The slope of the 2D IR spectra of the HOH bend is shown by the blue line in Fig. 2. It should be noted here that the initial slope of the HOH bend is about half of that of the OH stretch indicating that the frequency fluctuation of the HOH bend is significant even at $T = 0$ fs. Figure 2 also exhibits an initial decay with a time constant of ∼60 fs. The slope is almost constant from 100 to 150 fs and decays with a time constant of ∼120 fs after $T = 150$ fs.

Figures 3(a) and 3(b) show the stimulated photon echo signal, $S_{\rm PE}(\tau, T) \propto \int_0^\infty dt |P_{\rm I}^{(3)}(\tau, T, t)|^2$, of the OH stretch and the HOH bend. Known as three-pulse stimulated photon echo peak shift, the value τ of the maximum $S_{\rm PE}$ at a given waiting time T is related to the extent of the presence of the frequency correlation. The peak shift decays with increasing T due to the loss of the initial inhomogeneity.[46] The $S_{\rm PE}$ of the OH stretch at $T = 0$ fs has a maximum intensity at $\tau = 38$ fs. The peak shift of the OH stretch behaves in a similar way with the slope of the 2D IR spectra of the OH stretch with increasing T: an initial decay with a time constant of ∼30 fs, a plateau from 50 to 100 fs, and a slow decay with a time constant of ∼140 fs.

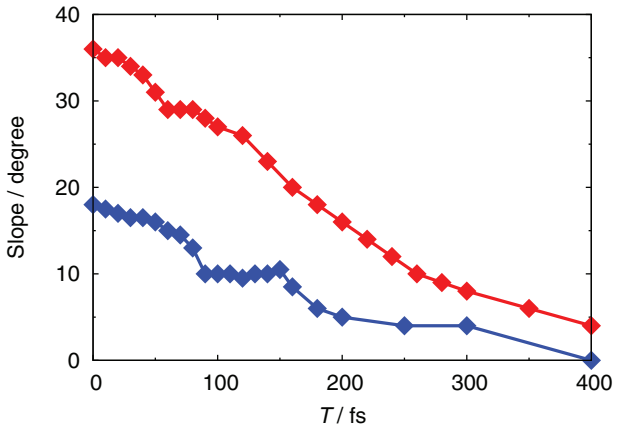

FIG. 2. Slope of the 2D IR spectra as a function of the waiting time, T, for the OH stretch (red) and the HOH bend (blue).

The $S_{\rm PE}$ of the HOH bend at $T = 0$ fs shows a larger peak shift of 53 fs when compared to that of the OH stretch. This is due to the smaller frequency fluctuation, $\langle \delta\omega^2 \rangle$, in the HOH bend than in the OH stretch. The peak shift clearly shows an initial decay with a time constant of ∼70 fs, followed by a plateau from 100 to 150 fs and a slower decay with a time constant of ∼120 fs, similar to the waiting time dependence of the slope of the 2D IR spectra of the HOH bend.

The time evolution of the OH stretch and HOH bend frequencies along the equilibrium MD trajectories are examined using normal mode analysis to elucidate the molecular origins of the fast frequency fluctuation of these motions. Figures 4(a) and 5(a) show the spectra of the frequency fluctuation of the OH stretch and the HOH bend, viz.,

$$\tilde{C}_\alpha(\omega) = \int dt \cos(\omega t) \left\langle \sum_i \delta\omega_{i\alpha}(t)\delta\omega_{i\alpha}(0) \right\rangle, \quad (10)$$

$$\delta\omega_{i\alpha}(t) = \omega_{i\alpha}(t) - \langle \omega_{i\alpha} \rangle, \quad (11)$$

where $\omega_{i\alpha}$ is the normal mode frequency of mode α, e.g., the OH stretch or the HOH bend of molecule i. Each mode is assigned to the molecule with the largest contribution. The averages of the largest contributions to the OH stretch and the HOH bend amount to ∼0.6 and ∼0.4, whereas the cumulative contributions within the first hydration shell are ∼0.8 and ∼0.5 for the OH stretch and the HOH bend, respectively.[28] The contributions of other molecules are, thus, much smaller than the largest contributions, which amount to ∼0.4 (∼0.6) for the HOH bend (OH stretch).

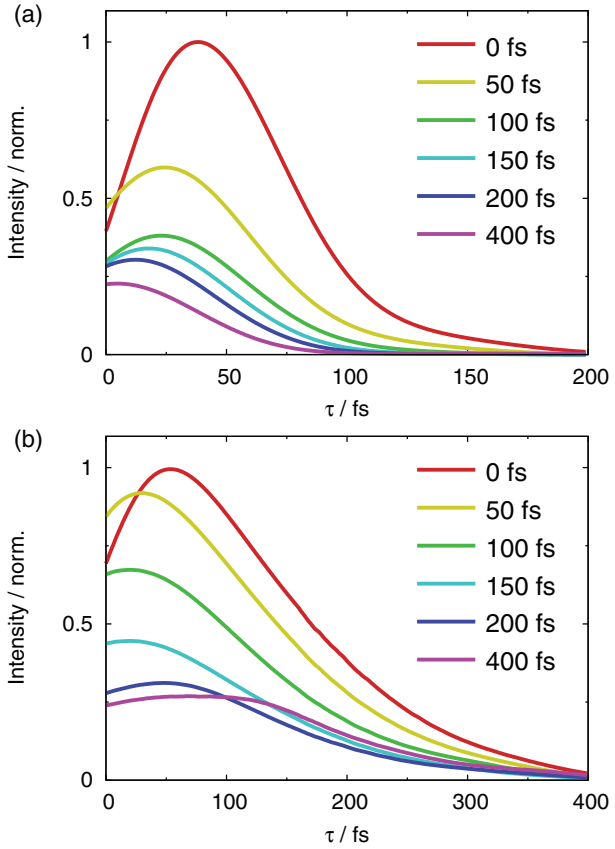

FIG. 3. Stimulated photon echo signals of (a) the OH stretch and (b) the HOH bend at different waiting times.

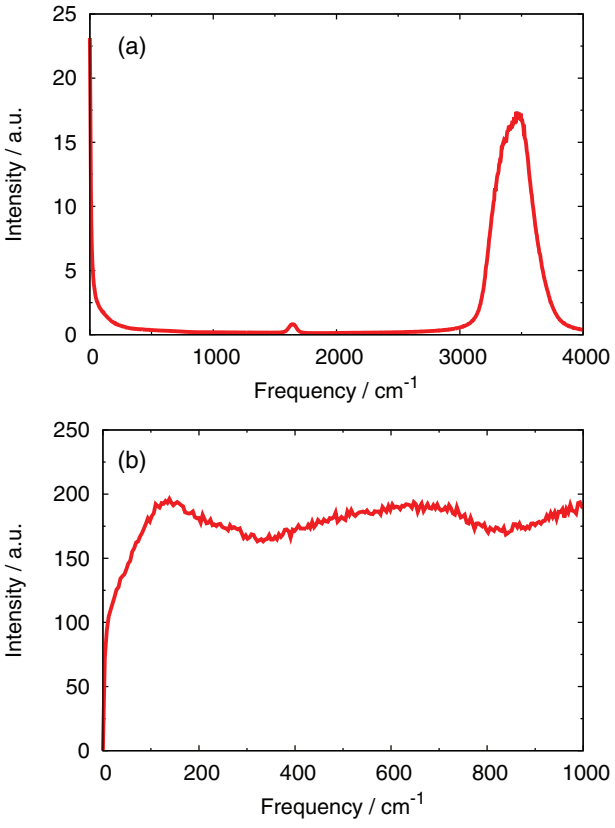

FIG. 4. Spectra of the frequency fluctuation of the OH stretch: (a) $\tilde{C}(\omega)$ and (b) $\omega\tilde{C}(\omega)$.

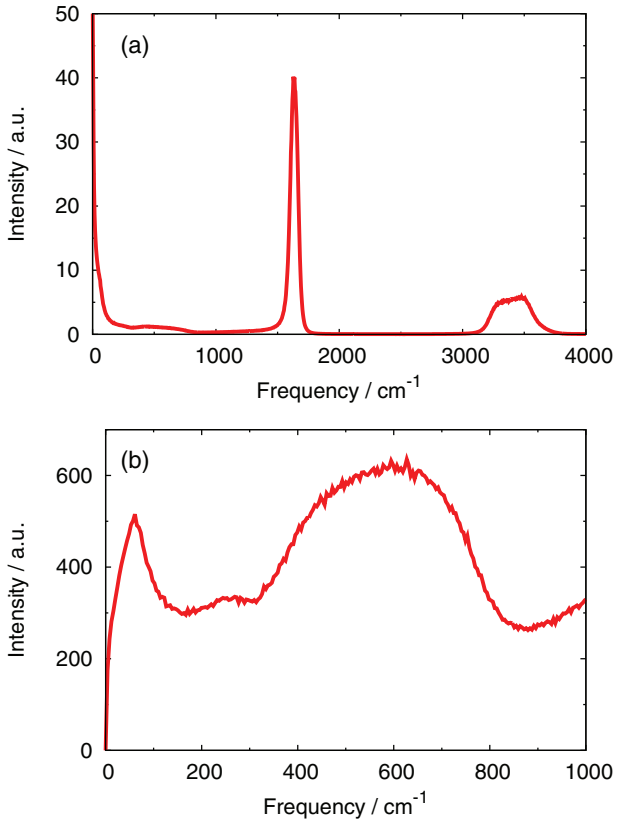

FIG. 5. Spectra of the frequency fluctuation of the HOH bend: (a) $\tilde{C}(\omega)$ and (b) $\omega\tilde{C}(\omega)$.

The frequency fluctuation of the OH stretch shows a strong peak at 3500 cm^{-1} due to the anharmonicity of the OH stretch (Fig. 4(a)). It is noted that the frequency of the OH stretch fluctuates due to the underlying intra- and intermolecular anharmonic dynamics of the system, though the frequency is calculated using the normal mode analysis. As shown in Figure 4(b), which emphasizes the contribution of the low frequency intermolecular motions, the spectrum of the OH stretch has a strong peak at ∼150 cm^{-1} due to the intermolecular HB stretch. It has been previously shown that the frequency fluctuation of the OH stretch in liquid D_2O is correlated to the fluctuation of the oxygen-oxygen distance.[13] The spectrum of the OH stretch also indicates the coupling between the OH stretch and the librational motion at ∼700 cm^{-1}.[13] In contrast to the peaks of the OH stretch and intermolecular motions, the peak at 1600 cm^{-1} is much weaker, indicating that the frequency fluctuation of the OH stretch caused by the HOH bend is negligible.

The spectrum of the frequency fluctuation for the HOH bend shows a strong peak at 1600 cm^{-1} due to the anharmonicity of the HOH bend (Fig. 5(a)). The peak in the 3000–4000 cm^{-1} region originates from the coupling between the HOH bend and the OH stretch. As seen in Figure 5(b), the frequency fluctuation of the HOH bend is also induced by the intermolecular HB bend at ∼60 cm^{-1}, whereas the coupling between the HOH bend and the intermolecular HB stretch at ∼200 cm^{-1} is weak. The present result shows that the frequency fluctuation of the HOH bend is due to the coupling between the HOH bend and the OH stretch and the

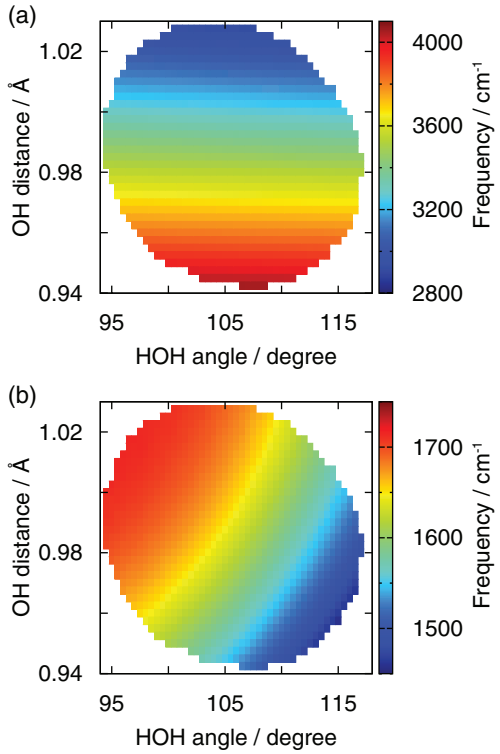

FIG. 6. Relationship between the intramolecular structure and the normal mode frequencies of (a) the OH stretch and (b) the HOH bend of liquid water. A C_{2V} structure is assumed for the water molecule and the plotted area covers 90% of water molecules with nearly C_{2V} symmetry in liquid water.

intermolecular HB bend. Furthermore, $\tilde{C}(\omega)$ of the HOH bend, considering only the coupling between the HOH bend and the OH stretch, shows that the plateau of the frequency correlation of the HOH bend mainly arises from the coupling between the HOH bend and the OH stretch. That is, the fluctuation of a HB can be probed through the coupling between the HOH bend and the OH stretch.

The above results suggest that the frequency fluctuation of the OH stretch is caused by the intermolecular HB stretch and the libration, while that of the HOH bend by the OH stretch as well as the intermolecular HB bend. Finally, we analyzed the reason why the frequency of the HOH bend is modulated by the OH stretch, but that of the OH stretch is not by the HOH bend. To elucidate the mechanism of the frequency fluctuation of the HOH bend caused by the OH stretch, we examined how the intramolecular structure affects the normal mode frequencies of the OH stretch and the HOH bend in liquid water. As seen in Figures 6(a) and 6(b), the frequency of the OH stretch depends almost only on the OH distance, whereas that of the HOH bend indeed depends on both the HOH angle and the OH distance. As a result, the frequency fluctuation of the HOH bend is caused by the coupling of the OH stretch, but that of the OH stretch is not significantly affected by the HOH bend.

IV. CONCLUSIONS

In the present study we investigated the frequency fluctuations of the OH stretch and the HOH bend in liquid water from MD simulations with the TTM3-F *ab inito*-based potential. The 2D IR spectra and peak shifts of the OH stretch and HOH bend were calculated directly from the third-order response function, for which only the high temperature approximation is used.

The 2D IR spectrum of the OH stretch at the waiting time $T = 0$ fs is diagonally elongated because of the strong correlation between ω_1 and ω_3. The calculated decrease in the diagonal width and corresponding increase in the anti-diagonal width with increasing waiting time are due to the loss of the initial inhomogeneity. The slope of 2D IR spectra of the OH stretch in liquid water suggests three processes, i.e., an initial decay with a time constant of ∼40 fs, a plateau from 60 to 100 fs, and a slow decay with a time constant of ∼180 fs, similar to those of the OH stretch in liquid D_2O, though these processes in liquid H_2O are faster than those in liquid D_2O. Normal mode analysis suggests that the frequency fluctuation of the OH stretch mainly arises from the intermolecular HB stretch and the librational motion.

The present calculation revealed that the ultrafast decay of the frequency correlation of the HOH bend, i.e., the 2D IR spectrum at $T = 0$ fs already leans towards the ω_1 axis. The frequency fluctuation of the HOH bend consists of three processes: an initial spectral diffusion with a time constant of ∼60 fs, a plateau from 100 to 150 fs, and a slow decay with a time constant of ∼120 fs. The time evolution of the normal mode frequency of the HOH bend along equilibrium MD trajectories reveals the strong couplings between the frequency of the HOH bend and the OH stretch as well as the intermolecular HB bend. Although the direct coupling between the HOH bend and the intermolecular HB stretch is not large, the effect of the intermolecular HB stretch, i.e., the fluctuation of the HB environment, via the OH stretch is seen as the plateau region from 100 to 150 fs in the time evolution of the slope of the 2D IR spectra and the peak shift. The present results demonstrate that the coupling between the HOH bend and the OH stretch is essential to reproduce the correct properties of the HOH bend though the coupling can have minimal effect on the frequency fluctuation of the OH stretch.

ACKNOWLEDGMENTS

The authors thank Dr. T. Yagasaki for helpful discussions. The present study was supported by the Grant-in-Aid for Challenging Exploratory Research (Grant No. 23655020), the Grant-in-Aid for Scientific Research (Grant Nos. 22350013 and 25288011), the Strategic Program for Innovation Research (SPIRE), MEXT, and the Computational Material Science Initiative (CMSI). S.S.X. acknowledges the support of the U.S. Department of Energy (DOE), Office of Basic Energy Sciences, Division of Chemical Sciences, Geosciences, and Biosciences. Pacific Northwest National Laboratory (PNNL) is a multiprogram national laboratory operated for DOE by Battelle. The calculations were carried out using the computing resources at the Research Center for Computational Science in Okazaki.

[1]D. Eisenberg and W. Kauzmann, *The Structure and Properties of Water* (Clarendon Press, 1969).

[2]A. Rahman and F. H. Stillinger, J. Chem. Phys. **55**, 3336 (1971).
[3]I. Ohmine and H. Tanaka, Chem. Rev. **93**, 2545 (1993).
[4]T. Head-Gordon and G. Hura, Chem. Rev. **102**, 2651 (2002).
[5]I. Ohmine and S. Saito, Acc. Chem. Res. **32**, 741 (1999).
[6]E. T. J. Nibbering and T. Elsaesser, Chem. Rev. **104**, 1887 (2004).
[7]S. T. Roberts, K. Ramasesha, and A. Tokmakoff, Acc. Chem. Res. **42**, 1239 (2009).
[8]T. Yagasaki and S. Saito, Acc. Chem. Res. **42**, 1250 (2009).
[9]H. J. Bakker and J. L. Skinner, Chem. Rev. **110**, 1498 (2010).
[10]T. Yagasaki and S. Saito, Annu. Rev. Phys. Chem. **64**, 55 (2013).
[11]S. Mukamel, *Principles of Nonlinear Optical Spectroscopy* (Oxford University Press, Oxford, 1999).
[12]M. Cho, Chem. Rev. **108**, 1331 (2008).
[13]J. D. Evans, J. J. Loparo, C. J. Fecko, S. T. Roberts, A. Tokmakoff, and P. L. Geissler, Proc. Natl. Acad. Sci. U.S.A. **102**, 13019 (2005).
[14]J. B. Asbury, T. Steinel, K. Kwak, S. A. Corcelli, C. P. Lawrence, J. L. Skinner, and M. D. Fayer, J. Chem. Phys. **121**, 12431 (2004).
[15]J. J. Loparo, S. T. Roberts, and A. Tokmakoff, J. Chem. Phys. **125**, 194522 (2006).
[16]K. Ramasesha, S. T. Roberts, R. A. Nicodemus, A. Mandal, and A. Tokmakoff, J. Chem. Phys. **135**, 054509 (2011).
[17]M. L. Cowan, B. D. Bruner, N. Huse, J. R. Dwyer, B. Chugh, E. T. J. Nibbering, T. Elsaesser, and R. J. D. Miller, Nature (London) **434**, 199 (2005).
[18]D. Kraemer, M. L. Cowan, A. Paarmann, N. Huse, E. T. J. Nibbering, T. Elsaesser, and R. J. D. Miller, Proc. Natl. Acad. Sci. U.S.A. **105**, 437 (2008).
[19]C. P. Lawrence and J. L. Skinner, J. Chem. Phys. **118**, 264 (2003).
[20]B. Auer, R. Kumar, J. R. Schmidt, and J. L. Skinner, Proc. Natl. Acad. Sci. U.S.A. **104**, 14215 (2007).
[21]D. Laage, G. Stirnemann, F. Sterpone, and J. T. Hynes, Acc. Chem. Res. **45**, 53 (2012).
[22]A. Paarmann, T. Hayashi, S. Mukamel, and R. J. D. Miller, J. Chem. Phys. **128**, 191103 (2008).
[23]A. Paarmann, T. Hayashi, S. Mukamel, and R. J. D. Miller, J. Chem. Phys. **130**, 204110 (2009).
[24]T. L. C. Jansen, B. M. Auer, M. Yang, and J. L. Skinner, J. Chem. Phys. **132**, 224503 (2010).
[25]J. Jeon, A. E. Lefohn, and G. A. Voth, J. Chem. Phys. **118**, 7504 (2003).
[26]G. S. Fanourgakis and S. S. Xantheas, J. Chem. Phys. **124**, 174504 (2006).
[27]G. S. Fanourgakis and S. S. Xantheas, J. Chem. Phys. **128**, 074506 (2008).
[28]S. Imoto, S. S. Xantheas, and S. Saito, J. Chem. Phys. **138**, 054506 (2013).
[29]T. Yagasaki, J. Ono, and S. Saito, J. Chem. Phys. **131**, 164511 (2009).
[30]S. Mukamel and J. B. Maddox, J. Chem. Phys. **121**, 36 (2004).
[31]T. Hasegawa and Y. Tanimura, J. Chem. Phys. **125**, 074512 (2006).
[32]T. L. C. Jansen, K. Duppen, and J. G. Snijders, Phys. Rev. B **67**, 134206 (2003).
[33]F. Paesani, S. Iuchi, and G. A. Voth, J. Chem. Phys. **127**, 074506 (2007).
[34]S. Habershon, G. S. Fanourgakis, and D. E. Manolopoulos, J. Chem. Phys. **129**, 074501 (2008).
[35]F. Paesani, S. S. Xantheas, and G. A. Voth, J. Phys. Chem. B **113**, 13118 (2009).
[36]F. Paesani and G. A. Voth, J. Phys. Chem. B **113**, 5702 (2009).
[37]F. Paesani, S. Yoo, H. J. Bakker, and S. S. Xantheas, J. Phys. Chem. Lett. **1**, 2316 (2010).
[38]J. Liu, W. H. Miller, G. S. Fanourgakis, S. S. Xantheas, S. Imoto, and S. Saito, J. Chem. Phys. **135**, 244503 (2011).
[39]H. Partridge and D. W. Schwenke, J. Chem. Phys. **106**, 4618 (1997).
[40]B. T. Thole, Chem. Phys. **59**, 341 (1981).
[41]M. Khalil, N. Demirdöven, and A. Tokmakoff, Phys. Rev. Lett. **90**, 47401 (2003).
[42]A. Sakurai and Y. Tanimura, J. Phys. Chem. A **115**, 4009 (2011).
[43]Y. Nagata and S. Mukamel, J. Am. Chem. Soc. **132**, 6434 (2010).
[44]T. Ishiyama, V. V. Sokolov, and A. Morita, J. Chem. Phys. **134**, 024509 (2011).
[45]N. Huse, S. Ashihara, E. T. J. Nibbering, and T. Elsaesser, Chem. Phys. Lett. **404**, 389 (2005).
[46]M. Cho, J. Yu, T. Joo, Y. Nagasawa, S. A. Passino, and G. R. Fleming, J. Chem. Phys. **100**, 11944 (1996).